Thermoplastic elastomer with advanced hydrophilization and bonding performances for rapid (30 s) and easy molding of microfluidic devices

Julie Lachaux, Clara Alcaine, Blanca Gomez-Escoda, Cecile M. Perrault, David Olea Duplan, Pei-Yun Jenny Wu, Inaki Ochoa, Luis Fernández, Olaf Mercier, Damien Coudreuse, et al.

Thermoplastic elastomer with advanced hydrophilization and bonding performances for rapid (30s) and easy molding of microfluidic devices

Julie Lachaux,[1] Clara Alcaine,[2] Blanca Gómez-Escoda,[3] Cécile M. Perrault,[4,5] David Olea Duplan,[6] Pei-Yun Jenny Wu,[3] Iñaki Ochoa,[2] Luis Fernandez,[2] Olaf Mercier,[7] Damien Coudreuse[3] and Emmanuel Roy*[1]

One of the most important area of research in microfluidic technologies focuses on the identification and characterisation of novel materials with enhanced properties and versatility. Here we present a fast, easy and inexpensive microstructuration method for the fabrication of novel, flexible, transparent and biocompatible microfluidic devices. Using a simple hot-press, we demonstrate the rapid (30s) production of various microfluidic prototypes embossed in a commercially-available soft thermoplastic elastomer (sTPE). This styrenic block copolymer (BCP) material is as flexible as PDMS and as thermoformable as classical thermoplastics. It exhibits high fidelity in replication using SU–8 and epoxy master molds in a highly convenient low-isobar (0.4 bar) and iso-thermal process. Microfluidic devices can then be easily sealed using either a simple hot plate or even room-temperature assembly, allowing them so sustain liquid pressure of 2 and 0.6 bars respectively. The excellent sorption and biocompatibility properties of the microchips were validated via a standard rhodamine dye assay as well as a sensitive yeast cell-based assay. The morphology and composition of the surface area after plasma treatment for hydrophilization purposes are stable and show constant and homogenous distribution of the block nanodomains (~ 22° after 4 days). These domains, which are evenly distributed at the nanoscale, therefore account for a uniform and convenient surface at a "*microfluidic scale device*". To our knowledge, this is the first thermoplastic elastomer material that can be used for fast and reliable fabrication and assembly of microdevices while maintaining a high and stable hydrophilicity.

.

1. Introduction

To ensure the successful application of microfluidics in different domains, the advent of optimized materials for microfabrication is still a major issue and an area of intense investigation.[1-3] The current difficulties to perform rapid prototyping of microfluidic chips for biological and biomedical research at a low level of investment remains a major bottleneck for taking advantage of these technologies and to promote innovation in the life sciences.[4,5] Indeed, these research areas require intense workloads for protocol validation and robust data acquisition. Furthermore, pre-clinical research is an essential aspect of the development of novel therapies, and very few research laboratories can rapidly integrate the inherent challenges of microfabrication. Therefore, at the levels of both research and commercialization, the lack of optimized solutions for biochip construction is a detrimental limiting factor.[6-8]

Beyond silicon, glass, and SU–8 photoresist materials, which use mainly relies on photolithography and etching processes, it is established that above a threshold, the thermoforming of polymer chips is the favoured approach for building microdevices. Indeed, even though impressive microfabrication processes have been reported with micromilling, 3D printing and paper-based technologies, these serial fabrication methods remain slow, often complicated, and their resolution and practibility limited.[9,10] In the last 15 years, thermoforming of polymers has therefore taken a leading role for rapid prototyping and manufacturing perspectives. In addition to their microstructuration capabilities, these polymers

[1] Centre Nanosciences et Nanotechnologies, CNRS UMR9001, Paris-Saclay University, 91460 Marcoussis, France
[2] Aragón Institute of Engineering Research (I3A), University of Zaragoza, Biomedical Research Network Center in Bioengineering, Biomaterials and Nanomedicine (CIBER BBN), Aragon Institute of Biomedical, Spain
[3] Institut de Génétique et Développement de Rennes, CNRS UMR 6290, Rennes, France
[4] Department of Mechanical Engineering, University of Sheffield, Sheffield, United Kingdom
[5] Insigneo Institute of in-silico medecine, University of Sheffield, Sheffield, United Kingdom
[6] Alphasip Inc., 44 Carretera de Fuencarral, 28108 Alcobendas, Madrid Spain
[7] Research and Innovation Unit, Inserm UMR-S 999, Marie Lannelongue Hospital, Paris-Saclay University, Le Plessis Robinson, France
*Corresponding author : *royemmanuel@live.com*

offer a broad range of physical and surface chemical properties through adaptable formulations, as well as an enriched panel of surface modification strategies by chemical treatments.[11,12] To date, a preferred and well-established method is the soft lithography (*SL*) of polydimethylsiloxane (PDMS).[13,14] The fabrication of microfluidic devices based on PDMS is an easy and robust approach, and the simplicity of PDMS manipulation has been key in its success. Indeed, with minimal training and equipment, the microfabrication of PDMS chips can be performed by non-experts without stringent methodological constraints. The robustness of such microsystems is illustrated by the famous statement from G. Whitesides of Harvard University: "One reason why people like PDMS is that it doesn't break". However, the use of PDMS remains a matter of intense debate, as reported by R. Mukhopadhyay,[15] in a publication entitled "When PDMS isn't the best", and its biological pertinence for cellular studies, as discussed by Berthier and colleagues in the paper "Engineers are from PDMS-land, Biologists are from polystyrenia"[16] is a constant subject of concerns. Among others, there are four major properties of PDMS that have specific negative impacts: 1) channel deformation due to its high mechanical compliance,[17] 2) evaporation, sorption and gas permeability,[18-20] 3) leaching-out of uncrosslinked oligomers,[21,22] and 4) hydrophobic recovery[23,24]. In addition, the use of *SL* for the rapid microfabrication of a large number of biochips requires a number of essential phases. These include several mixing and degassing steps for 5–15 min each, and a final curing treatment for typically 0.5 to 48 hrs. Therefore, *SL* is a lengthy approach that has a negative impact on the timely feasibility of any project. Furthermore, the cost of uncured PDMS (50–200 $/kg) may also be an obstacle. Finally, it is also important to take into account the time-consuming bonding process, which is typically achieved by ozone/O_2–plasma/Corona and others thermal treatments.[24,25]

As alternatives to PDMS, thermoplastic materials such as polycarbonate (PC) and polystyrene (PS) have been identified as promising candidates for faster prototyping and subsequent commercial transfer.[26,27] Indeed, these materials are amenable for rapid thermoforming processes such as injection molding, roll-to-roll and hot-embossing techniques. Complementary to these materials, polymethylmethacrylate (PMMA)[28,29] and polyimide (PI),[30,31] which are extensively used in the semiconductor industry, as well as polycyclo-olefin (PCO),[32,33] complete the set of thermoplastics that can be employed in microfabrication. However, the main drawbacks of these materials in replacing PDMS are 1) the requirement for large initial investments in equipment, 2) the need of essential skills in polymer sciences and molding technologies, and the associated challenges for the production of robust, microstructured master molds that sustain the specific molding conditions, and finally 3) the use of solvent-based and other thermally-assisted bonding approaches, which are problematic for a number of applications in the life sciences as well as for the structural integrity of the microstructures.[34,35]

Bridging the gap between thermoplastics (TP) and silicone (i.e. PDMS), recently published work with transparent and biocompatible sTPE (soft thermoplastic elastomers) materials, which combine the ease of processing of TP with the elastomeric properties of elastomer rubber (e.g. PDMS), have demonstrated enhanced fabrication and assembly potential.[36-40] Indeed, Brassard *et al.*,[38] described the thermoforming of open through-hole microstructures on a sTPE sheet and its integration in a 3D microfluidic monolithic device for DNA and protein immobilization. More recently, a sTPE microfluidic CD system for a fully integrated genomic assay was reported,[40] and Borysiak *et al.*[41] demonstrated stable zeta potential over time using these materials. We have also explored sTPE material solutions for high temperature applications that support, for example, polymerase chain reaction-based amplification of DNA.[42] Finally, Sudarsan *et al.*,[43] presented the synthesis of a melt processable thermoplastic elastomer gel consisting of 10 to 66 wt% of sTPE mixed with mineral agents for microfluidic network fabrication. Interestingly, these results are based on the use of commercial and synthesized styrenic block copolymer (BCP) materials, which show various molecular compositions and morphologies for the polystyrene/ethylene-butylene blocks. However, while this allows for continuous tuning of their mechanical properties (from MPa

	PDMS	***TP***	***Glass***	***Si***	***sTPE***
Optical properties	++	+	+++	-	+
Young Modulus	1 to 50 MPa	0.1 to 10 GPa	50 to 70 GPa	150 GPa	1 to 100 MPa
Breaking Strain (%)	100 – 200	10 – 50	–	–	500 – 800
Forming cycle	slow	fast	slow	slow	fast
Ease of molding	++	-	n. a.	n. a.	++
Valuable materials molds	large	narrow	n. a.	n. a.	large
Gas permeability	high	moderate	low	low	High to moderate
Reversible bonding	yes	no	no	no	yes
Permanent bonding	plasma, thermal, etc..	difficult	difficult	difficult	standard TP or/and heating
Resolution (nm)	50	20	10	10	10 – 50
Multilayered and 3D	easy	difficult	difficult	difficult	easy
Costs	moderate	low	high	high	low

Table 1 Table comparing mechanical, microfabrication and assembly properties of PDMS, TP, glass, silicon and sTPE materials properties for microfluidic technology and biomicrofluidics applications.

to GPa ranges), it negatively impacts their bonding capabilities. Moreover, the composition of these materials displays significant amounts (from 5 up to 66 %) of additional additives such as plasticizers, oil and processing agents, which further alter their bonding efficiencies as well as their microfabrication and hydrophilization performances. A summary of the essential characteristics of PDMS, sTPE and hard TP (thermoplastic) materials is provided in Table 1.

In this study, we use and characterize a new sTPE that displays flexibility and transparency comparable to those of PDMS. We report the enhanced microfabrication capabilities of the patented composition of the Flexdym™ material[44] as well as its stable hydrophilization and sorption properties. We further demonstrate the ultrafast (30 s), non-vacuum-assisted, isothermal and isobaric molding technique of a 4-inch sTPE microfluidic device using a simple low-cost hot press. Mechanical and bonding performances are characterized and quantitatively measured. Through the fabrication of a flexible microfluidic skin-patch and of a microfluidic device integrating a capillary pump inspired from Delamarche work,[45] we present the generation of the first fully flexible and thermoplastic-based microfluidic system. The absorption properties and biocompatibility of the Flexdym™ formulation are reported through rhodamine dye assays as well as sensitive live-cell analyses. In addition, we investigate the quality and nanostructured morphology of the surface using the following methods: AFM surface composition, UV-vis spectra, molecule sorption properties, contact angle measurements, and optical and electronic microscopy experiments. Given the features of this sTPE and its ease of use in rapid thermoforming manufacturing technologies, this work highlights a seamless strategy that integrates a low-entry cost prototyping approach with further industrialization paths using the same material interface.

2. Materials and methods

2.1. sTPE microfabrication

SU–8 and epoxy molds were fabricated in order to investigate the molding performance for structure depths ranging from 30 to 250 µm. SU–8 molds were prepared by photolithography using GM1060 and GM1075 photoresists (Gersteltec, Pully, Switzerland) on a 4″ silicon (Si) wafer. In order to improve their mechanical stability, SU–8 molds were fabricated through a two-step process. First, an initial layer of photoresist of 3–5 µm thickness was spin-coated on the 4″ Si wafer, baked for 5 min at 95 °C, and then exposed to UV light without a photomask. The exposed wafer was then hard-baked for 10 min at 95 °C. The second lithography step was standard SU–8 microstructure fabrication. Photoresist of 30–250 µm thickness was spun on the top of the initial SU–8 layer. Soft and post-exposure bakes were performed according to the temperature set points using heating and cooling rates provided by the supplier.[46] For epoxy mold fabrication, the SU–8 master structure was first transferred to a PDMS mold by *SL*. The epoxy mold was then obtained by mixing the two epoxy material components at 65 °C (the resin FR–1080 Conapoxy® and the Conacure® hardener at a ratio of 100/83 by weight. Ellswoth, Pointoise, France) and casting the mixture over the PDMS structure. After a curing step (12 h at 80 °C), the PDMS was peeled-off, and a final annealing step of 2 h at 180 °C was performed. The backside of the epoxy molds were then micromachined to obtain a total mold thickness of 1–1.2 mm. Prior to molding with Flexdym™, SU–8 and epoxy molds were treated with a wet and vapor deposition process of a commercial product (Optool™ DSX from Daikin Industries) in order to apply a fluorinated anti-sticking coating. Thin Flexdym™ foils (0.7 and 0.3 mm thick) were purchased as square sheets of 5″×5″ (Blackholelab Inc., Paris) and were used as received (standard of biocompatibility tests: USP Class VI). Such sheets can be cut simply with scissors to accommodate any size and stored for later usage.

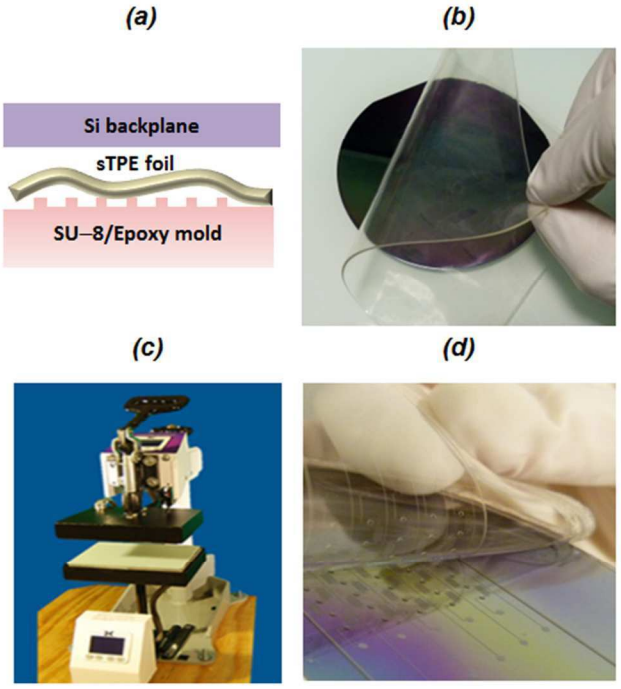

Figure 1 (a) Schematic of the stack for Flexdym™ isobaric and isothermal molding process. **(b)** Optical image showing the as-received Flexdym™ polymer and its manual positioning over the mold **(c)** Optical image of the simple micromolder kit for non-vacuum assisted, isobaric and isothermal molding process. **(d)** Easy and convenient peeled-off of sTPE foil from an SU–8 master mold (de-molding step).

For molding, we first used a high-performance Nanonex Ultra-100 hot-embossing/nanoimprint machine (NanoNex Inc., Monmouth, NJ, US), which allows for thermal molding under primary vacuum within a highly uniform imprinting pressure distribution. This equipment was used in order to investigate the upper and lower limits of the imprint pressure (1 and 34 bars) and the imprint temperature (100 and 190 °C). We then used a second cost-effective press consisting of a dual-side hot press equipped with a digital temperature controller. This system was used to determine the molding parameters in order to achieve high molding quality of microfluidic devices through an isothermal and non-vacuum assisted process. For both equipments, sTPE sheets were first gently pressed manually on the mold surface. Due to the intrinsic softness of the material, no damages were observed on the mold at this stage. Additionally, in order to

address the issue of trapped air bubbles in between the Flexdym™ and the mold structure, it is important to mention that any particular equipment or procedure been retained at the stage. Figure 1a and 1b illustrate respectively the composed stack for molding (a Si wafer treated with an anti-adhesive layer was positioned on the top of the sTPE) and the manual positioning of the flexible sheet. Figure 1c displays a photograph of the rapid micromolder kit (Blackholelab Inc., Paris). Embossing experiments were performed with an applied pressure of ~0.4 bar and an isothermal process of 120 and 180 °C for 120 s and 30 s, respectively. The typical zero shear viscosity of sTPE material is 3–6 orders of magnitude lower than that of hard TP, which explains the attractive processing conditions such as the short embossing time and low-pressure needed for replication.[47-49] Upon completion of the thermoforming process, the patterned elastomer sheet is removed from the mold as shown in Figure 1d.

2.2. Surface characterization and hydrophilization

In order to determine the block-copolymer phase distribution and the surface roughness properties over molding and hydrophilization experiments, atomic force microscopy (AFM) analyses were performed (Veeco Nanoman Dimension V microscope, Veeco, Mannheim, Germany). Both contact and tapping modes were operated under ambient conditions using high aspect ratio silicon nitride cantilevers. The block-copolymer phase distribution is an important parameter, as the polymer surface provides the interface that determines the interactions between the microstructures and all other microfluidic and biological environments and functions (i.e. wetting properties, adhesion, absorption, etc.). Borysiak *et al.*[37] previously reported time of flight secondary ion mass spectrometry experiments in order to determine the average PS block surface concentration for their solvent-assisted micromolding of styrenics BCP. Therefore, our AFM experiments aimed at determining the level of reproducibility and uniformity of the surface BCP distribution in order to confirm that the biphasic nature of the sTPE material is uniform at the scale of the microfluidic channels. Scanning electron microscopy (SEM) images were taken using a S-4800 scanning electron microscope operated at an acceleration voltage of 1.0–1.5 keV. Oxygen plasma treatments (Nextral NE10, Oerlikon, Pfäffikon, Switzerland) were conducted at a gas flow of 20 sccm, a pressure of 50 mTorr, with a power of 100 W for different times (2, 5 and 10 min). Static contact angle evolution over time was measured with a home-made goniometer platform and DI water as the probe liquid. Optical micrographs were taken using a Nikon Eclipse L150 optical microscope equipped with a QICAM fast digital camera from QImaging Corp.

2.3. sTPE prototypes: assembly, bonding and description

The mechanical properties of the sTPE (i.e 1.15 MPa) promote an intimate contact that occurs spontaneously across the entire surface when placed on a solid support or a similar Flexdym™ sheet (patterned or not). At this stage, this contact is reversible, and the sTPE layer can be peeled off and readjusted.

Additionally, when the surface was exposed to plasma, it was possible to proceed to the assembly of an entirely plasma-treated device without affecting the hydrophilization performance. This is due to the fact that the plasma exposure did not compromise the mechanical and viscoelastic properties of the material. This assembly procedure does not require any sophisticated equipment or others surface treatments. The actual bonding strength remains variable depending on the duration of contact and the temperature at which the assembly is performed. For monolithic (Flexdym™/Flexdym™) and hybrid (Flexdym™/glass) chips, we characterized the bonding strength through the two following approaches. First a Flexdym™ chip (monochamber design, one input/one output, 300 µm wide and 50 µm thick) was bonded to a PMMA manifold on one side and to either 1) a microscopy-grade glass coverslip or 2) a second Flexdym™ sheet on the other side. The assembled chips were then placed at room temperature or on a hotplate at 85 ºC for 5 min, 1 hour, or 12 hours. The strength of the bonding was measured by using a pressure control system (OB-1, Elvesys, France) to inject ultrapure water into these chips, whose outputs were blocked by a wax-sealed needle. Pressures that exceeded the bonding strength resulted in leaks through one of the layers of the assembled devices.

Two proof-of-concept microfluidic prototypes were fabricated. First, a skin-patch device was made out of two thin 300 µm thick Flexdym™ foils bonded together. One sheet featured a 200 µm wide, 50 µm deep and 20 mm long serpentine channel, while the second component was a flat layer. The thickness of the total patch, combined with its mechanical properties, resulted in a highly conformable contact with the skin surface. The patch (~20 cm^2) was manually positioned on the volunteer's forearm with gentle pressure. The adhesive characteristics of the sTPE soft block component have shown to provide enough support for the patch to hold in place. For further explanation regarding the tack properties of styrenics-based sTPE, we refer the readers to the following comprehensive reviews and publications.[50-52] Our second prototype involved a series of flexible capillary pump (*f-CP*) microfluidic devices. These systems were fabricated in order to investigate the hydrophilic properties of sTPE devices and to determine their capillary pumping performance. As proposed by Zimmermann *et al.*,[45] we selected an optimized design that comprises microstructured lines allowing a reliable filling behavior. The microstructures were rounded lines of 650 µm long and 150 µm wide, with a period of 800 µm in the perpendicular direction and 375 µm in the parallel direction. A half-period shift was introduced between successive rows. As the total area is 124.52 mm^2 and the system features a volume capacity of 72.7 %, the pump can accommodate, at its maximum, 1.25 µl of liquid for a depth of 10 µm. Six different depths (30, 50, 100, 150, 200 and 250 µm) of *f-CP* were fabricated from SU–8 and epoxy molds using 700 µm thick Flexdym™ foils and the micromolder kit equipment with a 30 s print time at 180 °C. The *f-CP* devices were then used, two days after been plasma treated for 10 min. Deionized water containing a dye was used for visualization in the experiments. The flow rate was determined based on the time required to completely fill a capillary pump.

2.4. Mechanical, sorption and biocompatibility properties

Mechanical analysis of extruded and molded Flexdym™ materials was performed with the standardized dogbone-shape sample along orthogonal directions to assess a possible structural anisotropy and to determine Young modulii values. All tests were performed according to the procedure described previously by Ochoa *et al.*.[53] Uniaxial tensile tests were performed under displacement control at a defined speed of 1 mm/min using an INSTRON 5848 microtester equipment (Instron Inc., Barcelona, Spain).

Two different investigations were performed in order to characterize and compare the adsorption and absorption properties of Flexdym™ and PDMS materials. The first test involved simple sorption measurements of rhodamine B (100 µM) within a straight microfluidic channel (50 × 50 µm^2) after 24 hrs of incubation. The rhodamine dye in the channel was imaged with a Zeiss Axio Observer Z1 fluorescent microscope equipped with a Thorlab DCU223 CCD camera. Image acquisition and analysis was performed using Micro-Manager 1.4 (open source microscopy software). The microchannels were then thoroughly rinsed with DI water and re-imaged to assess dye sorption in the material. The absorptive properties of Flexdym™ and PDMS were also tested using a more sensitive cell-based assay.[54] We used fission yeast cells whose proliferation is solely driven by a fusion protein between the cell cycle cyclin-dependent kinase Cdc2 and the cyclin B Cdc13.[55] For these experiments, DC450 cells (*h+ leu1::Pcdc13::cdc13-L-cdc2as::cdc13 3'UTR::ura4+ Δcdc13::NatMx6 Δcdc2::KanMx6 Δcig1::HygMx6 Δcig2::KanMx6 Δpuc1::Leu2+*)[54] were grown in minimal medium plus supplements (EMM6S) at 32 °C. These cells are sensitive to dose-dependent and reversible inhibition of Cdc2 activity by the ATP analog 3–MBPP1 (A602960, Toronto Research Chemicals Inc.). The 3–MBPP1 inhibitor was dissolved in DMSO at a stock concentration of 10 mM. For the absorption assay, 1 µM 3–MBPP1 or DMSO as a control were added to exponentially growing cells and 30 µl of the cultures were dropped on a glass coverslip or thin films of either Flexdym™ or PDMS. These setups were then incubated in a wet chamber at 32 °C for 3 hrs and subsequently imaged using a Zeiss Axio Observer (Carl Zeiss Inc.) equipped with a Hamamatsu Orca

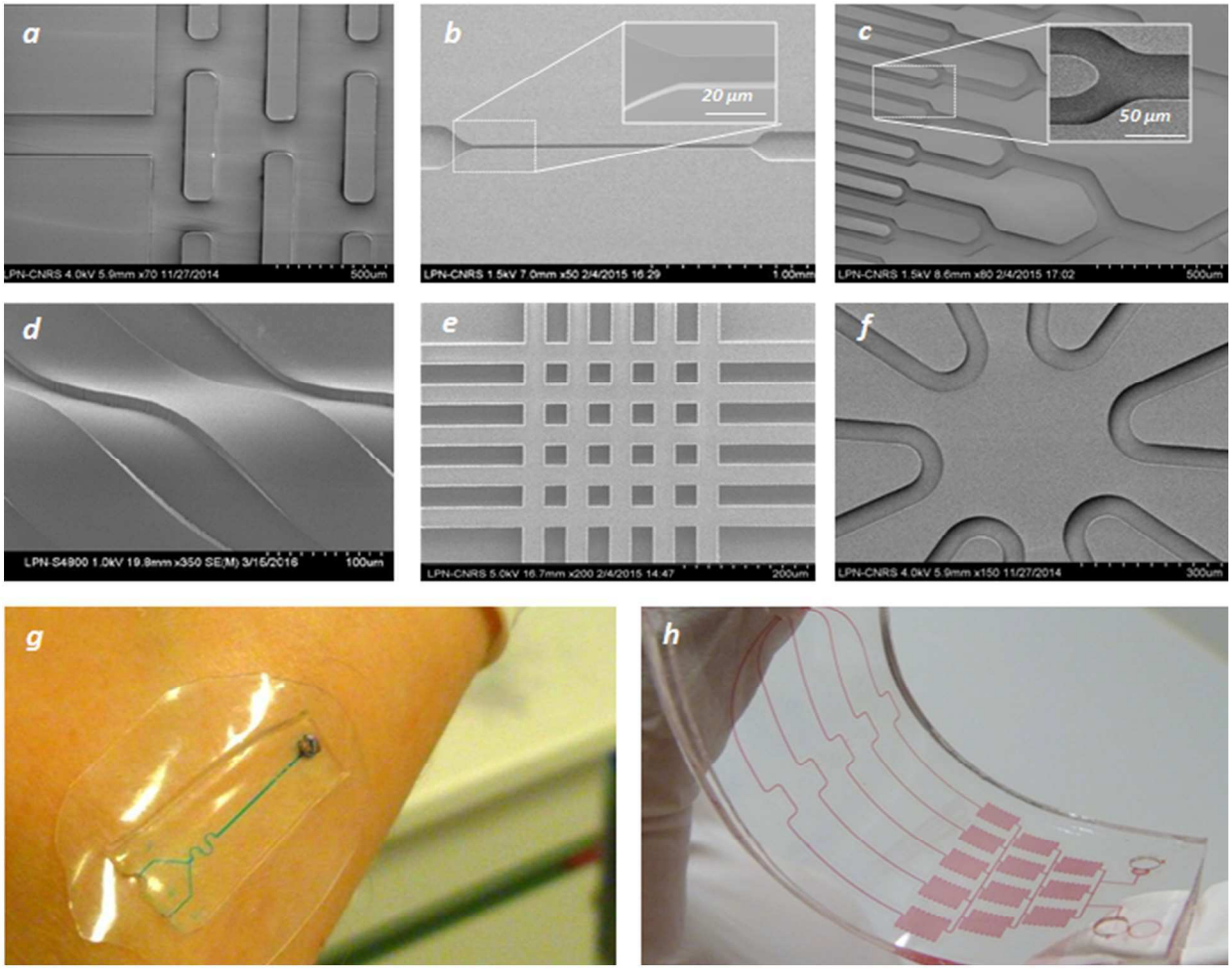

Figure 2. Series of SEM, optical, and photograph images illustrating the microstructuration and assembly performance of Flexdym™ material for various microfluidic devices. **(a)** Array of 150 µm wide, 650 µm long lines for the capillary pump demonstrator. **(b)** Isolated 20 µm wide channel connected to 200 µm channels, inserted close-up view displays the straight edges definition of molded structures. **(c)** Dense and branched network of microchannels from 200 to 50 µm wide, inserted close-up view of 50 µm wide channel. **(d)** Flexibility and edge definition of an array of 50 µm wide lines. (**e)** Dense and square interconnection of 30 µm lines. (**f)** Network of curved 40 µm wide channels. **(g)** Microfluidic skin-patch positioned on the experimenter's forearm. The total thickness is 700 µm, the microfluidic channel was filled with a blue food colorant. **(h)** Gradient like microfluidic generator network (25×75 mm^2 device) filled with a red food colorant.

Flash 4.0V2 sCMOS camera and driven by Visiview (Visitron GmbH, Puchheim, Germany). When appropriate, size at division was determined using Fiji (National Institutes of Health) and the Pointpicker plugin.

3. Results and discussion

3.1. sTPE microfabrication and device assembly

To structure Flexdym™ devices by hot embossing, we first used a Nanonex press, as it is regarded as one of the most precise and accurate system due to its air-cushion technology, which provides highly uniform pressure combined with vacuum at the imprinted interface. Focusing on 70 µm deep capillary pump structures, we determined the minimal imprinted time by performing a step-by-step approach, starting from 15 min imprints (results shown in Figure 2a-c). In accordance with the material properties and technical specifications of the Nanonex machine, we chose the following lower and upper limits for pressure and temperature: Pressure: 1 and 34 bars; temperature: 100 and 190 °C. The lower temperature limit was motivated by the fact that styrenic block copolymers display two glass transition temperatures (*Tg*): a low temperature for the ethylene/butylene (EB) soft blocks, and a higher one for the polystyrene (PS) hard blocks. The highest *Tg* is typically around 100 °C and corresponds to the service temperature of the material. For the soft blocks, the *Tg* is negative and provides the bonding capabilities (discussed in more details in section 3.4). The glass transition temperature of the PS block diverges from the neat polystyrene materials. This is due to some ‘‘lowering effect’’, interpreted as a consequence of premature molecular motion in PS domains induced by the poly(ethylene/butylene) segmental mobility, which consequently presents higher moldability.[56,57] Therefore, while molding hard TP materials (i.e., PMMA, PC, and PS) requires temperatures ranging from 140 to 220 °C, following $T_{emb} = Tg + 40–90$ °C as a rule of thumb, we found that the properties of sTPE in terms of viscosity and glass transition temperatures allowed a higher and wider range of molding operability. The results for four distinct sets of temperature and pressure conditions (S_i) are reported in Table 2. All experiments were indistinctly performed with epoxy or SU–8 molds. For all the assays, the applied pressure was released once the system cooled down to 55 °C. Both the total cycle time and the “plateau” ($t_{plateau}$) are reported ($t_{plateau}$ corresponding to the time for which both temperature and pressure maintained at their set values). Under the conditions S_1, (T_{emb}=190 °C, P_{print} = 1 bar), the required time for molding was 180 s. However, we observed that at this temperature, the cooling rate of the equipment was the limiting factor (cooling rate of 1.5 °C.s^{-1}), which restricted $t_{plateau}$ to ~ 55–60 secs. It is important to note that molding under such low pressure conditions presents new opportunities to explore alternative materials as master molds. Indeed, a number of materials were previously excluded from this procedure due to the requirement for high imprint pressures, such as 100 bar for PMMA molding[58] and 10–20 bar for PCO[59]. For example, epoxy mold deformation of up to 10% after 15 runs were reported.[60] Under the conditions S_2 (T_{emb}=100 °C, P_{print} = 34 bar), the overall cycle time was 165 s, with $t_{plateau}$ of ~ 70–75 secs. In this case, the limiting factor was the establishment of the imprint pressure, as the pressure rate was 1.2–1.3 bar.s^{-1}. Under the conditions S_3 (T_{emb}=190 °C, P_{print} = 34 bar) and S_4 (T_{emb}=140 °C, P_{print} = 1 up to 5 bar), the overall cycle time was 120 s. For both S_3 and S_4, $t_{plateau}$ were shorter, and equal 8–10 s and 20–24 s, respectively. Thus, compared to the S_1 and S_2 setups, perfect molding was obtained faster in this later series of conditions. At this point, the technical limitations of the equipment represent the main bottleneck for this fabrication process, but we anticipate that further optimization would permit even faster prototyping cycles. In previously described imprinting procedures, both temperature and pressure required significant time steps to set and cycle. For PCO materials, Cameroun *et al.*[59] reported a $t_{plateau}$ of 2 min (it is worth mentioning that in this study, the thermal ramps were lower and the structure depths were smaller than in our experiments). For PMMA microchip fabrication, Mathur *et al.*[61] used a total cycle time between 20 and 30 min. In contrast, our investigation shows that sTPE imprint cycle time can range from 120 to 180 s, and could potentially be even faster, as we were limited by the variotherm and variobar capabilities of our equipment.

Parameters	*Nanonex embossing*				*Heat press*	
Series	S_1	S_2	S_3	S_4	S_5	S_6
Vaccum support	yes	yes	yes	yes	no	no
Temperature (°C)	190	105	190	140	180*	120*
Pressure (Bar)	1	34	34	1-5	~0.4**	~0.4**
Overall cycle time (s)	180	165	120	120	30	120
Plateau time (s)	55–60	70–75	12–16	20–24	n. a.	n. a.

Table 2 Flexdym™ molding parameters for classical embossing investigation using Nanonex equipment (S_1, S_2, S_3 and S_4) and for isothermal(*) and isobaric(**) processes using the micromolder kit (S_5 and S_6).

To develop an isothermal and isobaric process, we used a much simpler kit molding equipment. As detailed previously, in this system, the stack (Figure 1a) is positioned between pre-heated plates and the press is manually operated with a handle (Figure 1c). The applied pressure is calibrated using a screw (stop course), while each temperature plate is independently regulated. A first series of tests (see S_5, Table 2) were done at T_{emb} = 180 °C and a pressure of ~0.4 bar. By progressively reducing the imprint times, starting at 5 min, we determined that an effective step of 30 s was sufficient to reproduce all tested microstructures with high quality and resolution. This 30 s isothermal and isobaric process was shown to perform very well for sTPE imprinting, as shown by SEM imaging (Figures 2d-f). High reproducibility of features ranging from 10 to 50 µm, at different array densities was demonstrated. Also, for geometries with high curvatures, no pull-off of material (a common issue with imprinting) was observed. Next, for a low-isothermal process at T_{emb} = 120 °C, we determined that a cycle time of 120 s was necessary for complete molding. While with PDMS and other liquid molding materials, imprinting must be

assisted with vacuum to reduce the formation of air bubbles, such problem was not observed. This was also confirmed both with optical (Figures 1d, 2g, h) and SEM imaging (Figure 2d-f). These observations can be explained by the relatively high gas permeability of the sTPE material at elevated temperatures. In crystallized state, PS nanodomains interrupt the gas flow and retard permeation at a higher rate than the soft and more permeable EB polymer blocks. Although sTPE materials are diverse in composition and morphology, the general range of permeability coefficients for nitrogen and oxygen gas at room temperature reported in the literature are 20–200 times lower than that of PDMS.[62,63] Importantly, using master molds that were coated with the Optool™ DSX anti-sticking reagent, we were able to reuse them several times without inducing any notable damage to the photoresist/epoxy features. We also observed that the molded surfaces were smooth and free of defects, with roughness values of 1.8 and 2.7 nm for SU–8 and epoxy molds, respectively. SEM inspection of the fluidic structures in the capillary pump systems proved the excellent fidelity of the sTPE patterning, which showed no apparent defects. We found no difference between imprints made using either of the fabrication conditions described above. In both cases, structures showed well-defined shapes and excellent surface qualities. None of the classical issues encountered for hard thermoplastics, such as edge damage and asymmetric pull-off of plastics in part due to interfacial friction between the polymer and the mold upon de-molding, were noticed.[64,65]

Due to the ability of Flexdym™ to perform conformable contact, monolithic devices can be easily mounted. The viscoelastic and rheological properties of the EB soft blocks also provide reversible up to irreversible (and cohesive) bonding properties to a broad range of solid supports without the requirement for heat and/or solvent treatments (see section 3.4).[40,66] Taking advantage of the microfabrication, bonding and mechanical properties of sTPE, we then generated a 600 µm thick microfluidic skin-patch device and a large gradient-like microfluidic generator network (25×75 mm^2). The conformability and adhesive properties of the material allowed the patch to stick easily onto the forearm's skin (Figure 2g), and to remain in place during common arm movements. To the best of our knowledge, this constitutes the first demonstration of fabrication and assembly of a microfluidic device exclusively using a thermoplastic elastomer. Compared to PDMS and classical hard thermoplastic materials, the extreme rapidity of manufacturing microfluidic devices with Flexdym™, from molding to assembly, opens novel opportunities for ground-breaking microfluidic systems. Importantly, the "soft" conditions involved in this process (no harsh chemicals, physiologically relevant temperatures, ambient pressure) is particularly well-suited for the development of devices targeted toward biotechnologies (cellular studies, molecular diagnostics, point of care systems). sTPE is also a material that is amendable for further industrial thermoforming technologies such as injection molding, and thus encourages a cycle in which successful prototypes can be rapidly transferred from research to commercial applications by using a single polymeric material throughout the entire process.

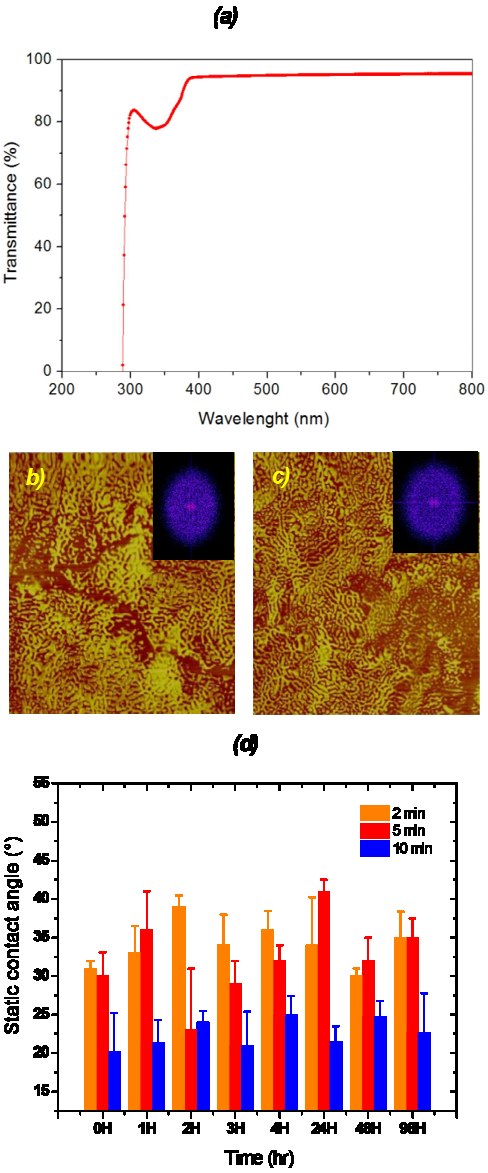

T_{100W} (min)	2 min	5 min	10 min
θ_{stat}(°)	34,0 ± 2,8	32,3 ± 5, 3	22,0 ± 1,8

Figure 3. (a) UV-vis spectra of Flexdym™ material. **(b)** Contrast phase AFM image of as molded Flexdym™ material. Hard block polymer components appear bright in surrounding elastomeric ethylene/butylene soft phase (brown). **(c)** Contrast phase AFM image of Flexdym™ material exposed to oxygen plasma (gas flow of 20 sccm, 100 W and 10 min). **(d)** Evolution of static contact angle of DI water for Flexdym™ treated with O_2 plasma (20 sccm, 50 mT and 100 W for 2, 5, and 10 min). Values are averages from five measurements; standard deviations are below ±5.

3.2. Optical, hydrophilization and surface properties

Optical or fluorescence measurements in a fluidic chip require the use of materials that show a high level of transparency, primarily in the UV and visible range. Flexdym™ fulfills these conditions, as shown in Figure 3a. Indeed, it reaches the limit of 50% transmittance (which we considered to be an

acceptable limit in transparency) at a wavelength of 295 nm. Depending on the specific grades of PMMA and PCO, this 50% threshold was reached between 275 and 365 nm,[67] demonstrating that Flexdym™ features similar properties to the clearest materials. This transparency window is sufficiently wide for a large number of fluorophores, particularly the most popular fluorescent Cy3 and Cy5 dyes, which have excitation wavelengths at 550 and 650 nm and emission wavelengths at 570 and 670 nm, respectively. As a BCP, Flexdym™ is a clear material because PS hard block domains are too small (e.g. 10–30 nm) to scatter light.

As block copolymer materials, Flexdym™ and other similar sTPE are biphasic materials, which comprise different monomer sequences that are distributed in nanoscale domains.[52] Therefore, the question of surface homogeneity (or the level and amplitude of heterogeneity) is of importance for estimating the qualitative uniformity of the microfluidic interface. Figure 3b displays a typical AFM phase image of 1×1 μm^2 area of the molded surface. The bright areas were attributed to the block copolymer component with higher modulus (i.e. PS) surrounded by the brown rubber matrix of ethylene-butylene.[68,69] The inserted fast Fourier transformation (FFT) displays a circular ring, which confirmed that the pattern had a uniform average wavelength and that the equilibrium morphology (effective segregation) of the surface was isotropic. Moreover, this morphology appeared to be uniform at a scale pertinent to a microfluidic system. Indeed, we can reasonably envisage that a meniscus or a liquid element will interact within an averaged fashion with the contacted surface. This is therefore our assumption for a homogenous surface at a *microfluidic device scale* level. We also report the evolution of the same surface after it has been treated by the most constraining plasma exposure (i.e. 10 min/200 W). Figure 3c reveals a similar surface morphology compared to the molded surface, with an identical "spaghetti-like" network of nano-sized PS regions. PS domains were evenly spread over the entire scanned area. The inserted FFT image also features an annular ring, confirming the uniform average patterns. Unlike plasma exposure of PDMS, which results in the formation of a thin but rather brittle silica layer that tends to generate cracks,[70,71] the plasma-treated sTPE surface keeps its structural integrity and does not compromise mechanical and viscoelastic properties, allowing for intimate contact upon device assembly. These data show that plasma exposure affects neither the surface morphology nor the block copolymer distribution, suggesting that even after an intense plasma treatment, the surface morphology meets the criteria for a homogeneous surface at a microfluidic device scale. These results were confirmed for every implemented plasma treatment and also for all molded parts produced at 180 °C using the kit molder equipment, independently of the mold materials.

Pristine surfaces of Flexdym™ material are hydrophobic and exhibit advancing and receding contact angles of 105 ± 4° and 88 ± 4°, respectively. Given that the soft EB phase is the dominant matrix and that polyethylene (PE) and polybutylene (PB) have advancing contact angles of 97° and 112° respectively, while PS has a lower advancing angle of 91–94°, this average measured value for the Flexdym™ material is consistent with our AFM investigation. This hydrophobicity implies that active pumping would be required for fluidic manipulation of aqueous solutions. Therefore, we investigated treatment of sTPE with O_2-plasma and followed the evolution of the statistic contact angle ($\theta_{stat.}$) using DI water over a period of 4 days after 2, 5 and 10 min exposure times (Figure 3d). Plasma treatment of EB and PS phases are accompanied by the conversion of hydrocarbon units into hydrophilic groups such as carboxylic acid. The density of functional groups and hence the wetting properties of the resulting surfaces generally depend on the plasma conditions, for which a detailed investigation has yet to be performed. For 2 and 5 min exposure times, Figure 4b shows that a stable hydrophilization was obtained over a period of 4 days, and the average measured values over this period were 34.0 ± 2.8° and 32.3 ± 5.3°, respectively. Increasing the plasma exposure to 10 min improved the hydrophilicity, and an average value of 22.0 ± 1.8° was obtained. Compared to the well-known hydrophobicity recovery of PDMS surfaces, this result represents a significant asset for various microfluidic applications. Both PDMS and EB soft blocks feature a negative *Tg*, which is an essential criteria for their conformable contact and elastomeric abilities ($T_{g,PDMS}$ = ~ –120 °C and $T_{g,EB}$ = ~ – 50 °C). A negative *Tg* also underlines the ability of the polymer chains to move and diffuse above this temperature, and this is one reason for the hydrophobic recovery of PDMS at room temperature. In addition, for PDMS, the significant and fast hydrophobic recovery is also related to the mobility of un-crosslinked oligomers. However, for EB soft blocks, the situation is different. Indeed, soft EB are covalently linked to the PS hard domains. Thus, the mobility of the EB flexible chains are restricted through their attachment to

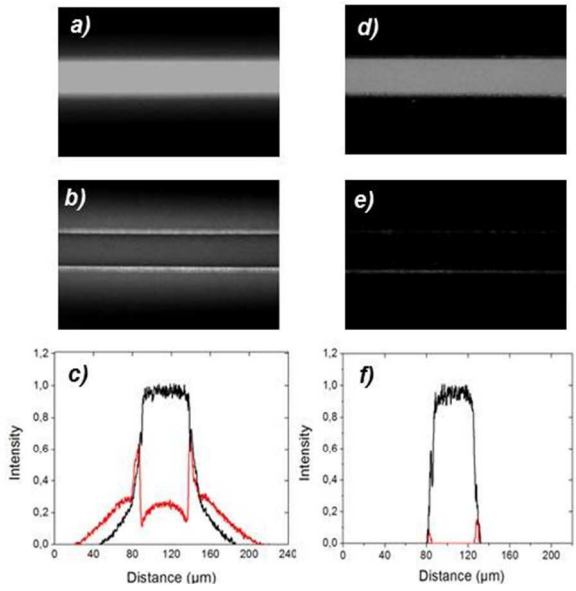

Figure 4. Rhodamine B adsorption and absorption studies. Images **a)** and **d)** show the absorption of 100 µM Rhodamine B (24 h incubation) in 50 µm wide channels fabricated from PDMS and Flexdym™ respectively. Images **b)** and **e)** show PDMS and Flexdym™ adsorption and leakage after rinsing with DI water. The corresponding intensity profiles show the normalized fluorescence intensity for PDMS and Flexdym™ in **c)** and **f)** respectively (black and red lines correspond to 24 h incubation and after rinsing, respectively).

the thermally stable PS blocks ($T_{g,PS}$ = ~ 100 °C), providing the reported stability.

3.3. Sorption properties and biocompatibility

The tendency of PDMS to sorb small hydrophobic molecules is a well-known issue and represents an important obstacle for its use in a number of assays. In particular, it makes PDMS incompatible with a host of biological applications that involve manipulation and/or delivery of small molecules as well as maintenance of a constant nutritional state for living cells.[72] Surface modification treatments such as sol-gel and paraffin coating or parylene deposition have been proposed to circumvent this limitation. However, their implementation furthers complexifies the fabrication and assembly processes.[73-75] The sorption properties of PDMS are illustrated using a rhodamine assay in Figure 4a and 4b. In contrast, when rhodamine was flown in a Flexdym™ chip and subsequently washed with DI water, we only detected a faint fluorescent signal at the sidewall of the channel (Figure 4d and 4e). The intensity of this signal could either represents a very limited level of absorption or an artifact linked to the intrinsic sidewall roughness. Nevertheless, compared to PDMS, this demonstrates the absence of significant absorption by Flexdym™, which is comparable to the situation with pure PS,[76] a favored material for cell culture. Altogether, this suggests that Flexdym™ is ideal for microfluidic bioreactors and organic chemistry applications (e.g. protein detection, pre-clinical drug candidate in-vitro testing). We then ascertained the absorptive properties of Flexdym™ using a cell-based assay, as our previous study demonstrated that the rhodamine test is not sufficiently sensitive to precisely evaluate this parameter.[54] To this end, fission yeast cells operating with an analog-sensitive fusion protein of the cell cycle cyclin-dependent kinase Cdc2 and the B-type cyclin Cdc13[55] were treated with 1 μM of the ATP analog 3–MBPP1 (a small hydrophobic molecule) and grown in contact with either a glass substrate, Flexdym™ or PDMS (see Materials and Methods). At this concentration of 3–MBPP1, the function of the analog-sensitive Cdc13–Cdc2 fusion is inhibited, leading to cell cycle arrest and elongation of the cells without division.[55] Absorption of the drug by the substrate reduces the effective concentration of 3–MBPP1 to which the cells are exposed, resulting in nuclear division and formation of the division septum. As expected, cells grown on glass in the presence of inhibitor did not divide, leading to a strong elongation phenotype (Figure 5). In contrast, on PDMS, cells kept dividing at a size similar to the untreated control cells, suggesting very strong absorption by this material. Importantly, while cells growing on Flexdym™ formed septa, this occurred at a much longer size than the control, reflecting only limited absorption of the drug. These results demonstrate that Flexdym™ performs significantly better than PDMS. Furthermore, we did not observe either morphological phenotypes or increased cell death in these experiments, supporting the biocompatibility of Flexdym™ for live-cell studies.

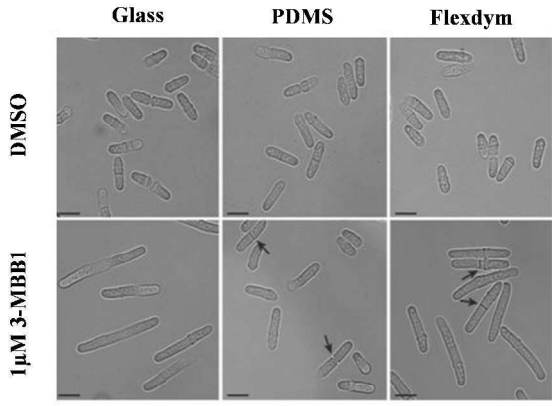

DMSO			1μM 3-MBB1		
Glass	PDMS	Flexdym	Glass	PDMS	Flexdym
14.9±0.4	15.4±0.6	15.1± 0.5	n.d.	15.9±0.1	26.6± 0.6

Figure 5. Flexdym™ shows significantly lower absorption of small hydrophobic molecules than PDMS. Fission yeast cells operating with an ATP analog-sensitive machinery for cell division were treated with 1 μM of the 3-MBPP1 inhibitor (or DMSO as a control) and incubated on different substrates for 3 h at 32 °C. Top panels: DIC images of cells in the different conditions. On glass, cells stop dividing, leading to elongation without division. On PDMS, strong absorption of the inhibitor results in cells dividing as in the DMSO control. Cells grown on Flexdym™ also keep dividing but at a much longer size, consistent with a reduced absorption of the drug. Arrows indicate division septa. Scale bar = 10 μm. Bottom table: cell size at division (in μm) as in the top panels. Averages of 3 independent experiments (n>100 for each experiment) with standard errors are shown. n.d.: not determined (cells do not divide in the presence of 1 μM 3-MBPP1 when grown on glass).

3.4. Mechanical and bonding properties

For organ-on-chip models of lung,[77] intestine[78] and other mechanically-driven organs, key physiological parameters, such as breathing, are generated by applying computer-assisted mechanical stimuli to the overall cellularized microfluidic environment. Thus, the mechanical properties (e.g. tensile modulus of elasticity, stress relaxation) of the material are critical criteria to develop functional organ-on-chip devices. We therefore carried out experiments to evaluate the effects of the fabrication process on the mechanical properties of Flexdym™ foils produced by extrusion and microstructured. Stress-strain experiments were analyzed in either the direction parallel or perpendicular to the direction of polymer flow regarding the extrusion process. For extruded foils, the Young's modulii were 1.30 ± 0.12 and 1.21 ± 0.13 MPa for parallel and perpendicular directions, respectively, while molded parts exhibited modulii of 1.13 ± 0.16 and 1.18 ± 0.18 MPa for similar directions. This corresponds to anisotropy parameters of 1.07 for the extruded and 1.04 for the molded parts. Mechanical anisotropy over extruded polymer foils is a well-known behavior that is intrinsic to the process, because of the planar elongational flow field imposed on the molten polymer thought the calibrated dye. For the extrusion of styrenic block copolymers, Lee and colleagues[79] reported that the anisotropy may also depend on the domain sizes and orientations, and they characterized an anisotropy factor of 10.2 for standard Kraton material. Similar value (i.e. 7.1) was obtained using a roll-milling process.[80]

Far beyond the scope of the current mechanical characterization, the size of the domains and their coalescence onto micro-domains are related to the primary polymer composition, the ratio of each block, and their relative

architectures (di-blocks, tri-blocks, star-blocks, etc…). In-depth description of these principles have been thoroughly reviewed.[81,82] For Flexdym™ composition, first, one can noticed the already reported homogeneous distribution of the nanodomains for both molded and plasma treated devices (see figures 3b & 3c), and second the reduced anisotropy of molded material compare to extruded one. Indeed, the soft embossing process (i. e. low temperature and low shear-stress vs. extrusion process), induced minimal shear-stress on the melted polymer, and it contributes to lower the internal stress, acting similarly to an annealing step. Finally, a 1.04 anisotropy factor and a reduced Young Modulus down to 1.15 MPa have been characterized, value comparable to PDMS material, contributed therefore to the important properties of soft, intimate and tight contact for devices assembly.

The bonding parameters and strength are two important criteria, especially when one aim to target biological species integration on chip, and it is a well-known drawback of current thermoplastic-based microfluidic systems. Indeed, intrinsically, classical thermoplastic materials need to be maintained in contact through a mechanical load (due to their rigidity) and the polymer chains at the interfaces need to be activated (either chemically or through a heating step) for bonding to occur. Therefore, in addition to the requirement for specific instrumentation, the use of such techniques requires severe controls and subtitle process developments in order to avoid structural deformation, which contributes to slow down the perspectives for biological reagent integration. To investigate the compatibility of Flexdym™ with the rapid fabrication of sealed devices, we characterized the bonding strength for both monolithic Flexdym™ and hybrid Glass/Flexdym™ microchips.

For monolithic devices, a 5 min bonding procedure at room temperature was not sufficient to support pressures above 200 mbar. However, a 1 h contact was suited for internal pressures up to 600 mbar. The bonding performances were drastically increased using a heat-assisted process. Indeed, devices sealed at 85 °C for 5 min and 1 h could be used with pressures up to 0.6 and 2 bar, respectively.

These results open the way for enhanced bonding solutions, covering the range of pressures commonly used in microfluidic experiments, in particular in the life sciences. Indeed, even when limited to 600 mbar, the bonding at room temperature provides a major advantage for anyone seeking for a rapid solution to seal a cellularized micro-environment. In addition, such pressure is sufficiently important for various organ-on-chip and others artificial organ applications. For example Potkay,[83] reported that the required driven pressure for a microfluidic clinical artificial lung handling physiological flow rates from 2 to 6 ml.min^{-1} should be limited to 10–110 mbar depending on the foreseen clinical setting. It should also be noted that at 85 °C, the polymer does not melt and is therefore not deformed, maintaining its structural integrity due to the presence of the hard blocks which feature a *Tg* below the bonding temperature. Thus, at this temperature, we simply enhance the macro-molecular motion and the re-organization/re-orientation of the soft polymer segments (i. e. $T_{g,soft} \leq -50$ °C) at the interface, contributing to the bonding.

For hybrid Glass/Flexdym™ devices, a 5 min bonding procedure at room temperature and 85 °C were not sufficient to support pressures above 200 mbar. However, a 1 hr bonding step made these devices compatible with up to 0.4 and 1 bar for room temperature and 85 °C bonding, respectively.

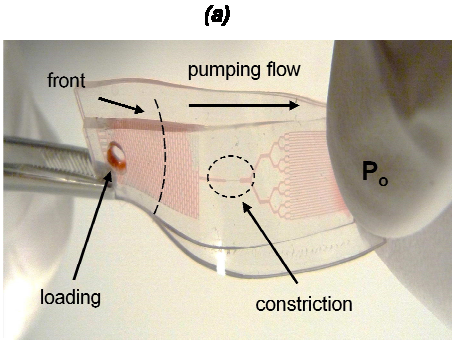

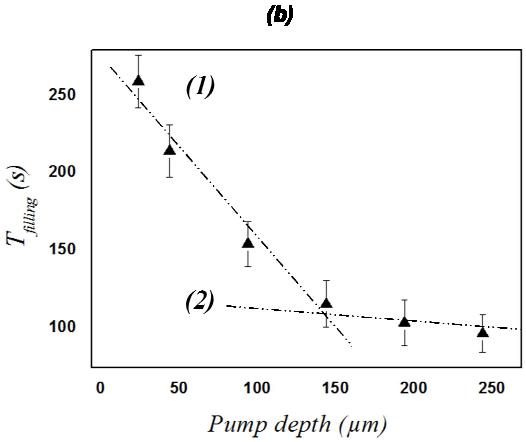

Pump Height h(µm)	Pumping rates (µl.s^{-1})
30	0.14
50	0.29
100	0.80
150	1.62
200	2.40
250	3.29

Figure 6 (a) Photograph of a monolithic thermoplastic elastomer flexible capillary pump device maintaining a high level and stable hydrophilicity over assembly. **(b)** Time to fill entirely the micropump area *vs*. the structure depth of the capillary pump. Two distinct trends are observed, line *(1)* linear, line *(2)* quasi-static trends. **(c)** Achievable pumping rate *vs*. the sturcture depth of the capillary pump.

3.5. Flexible capillary pumps

One of the main limitations of actuated microfluidic systems is their dependency on external power source for pumping purposes. A promising alternative is the passive capillary flow approach, making the system more portable and minimizing dead volumes. In such pumps, the fluid progresses as a filling front perpendicularly to the main axis of the chip and then enters a constricted microchannel area. This area acts as a flow resistor, and was specifically designed as a preferential

location to integrate molecular assays (Figure 6a). In our case, since we intended to assess the performance of the capillary pump when using Flexdym™ as a microfabrication material, we did not use this constricted area. The liquid was pipetted directly in the pump and the pumping performance was determined by the time necessary to fill the pump. This very efficient design, which is the result of years of optimization from the Delamarche group, was shown to exhibit a reliable filling behavior and to minimize the trapping of air bubbles in a very robust manner.[45,84,85] In our experiments, the filling and the advancing front were constant and reproducible over many assays. We measured $t_{filling}$ for six different series of capillary pumps (structure depth from 30 to 250 µm) *vs.* depth (Figure 6b). Two distinct regimes could be observed. For channels up to 150 µm deep, we found a quasi-linear relationship between $t_{filling}$ and the depth of the channel. This behavior is expected for rectangular cross-section channels where width >> height (here, the pump is 6.46 mm wide) and it was reported analytically by Berthier *et al.*[86] as an extension of the classical Washburn's equation[87] describing the capillary rise in straight capillary. For channels with depths greater than 150 µm, $t_{filling}$ appeared to be constant and independent of the specific pump's depth. This is due to the geometry and arrangement of the features within the capillary pump and to the associated fluid dynamics. For constrained flows, capillary pressure and Hagen-Poiseuille laws are preponderantly governed through their smallest dimension (considering solely dimensional parameters). Since the narrowest gap separating two microstructured lines is 150 µm (see section 2.3 prototype description), fluid flow is controlled by channel's depth as long as it remains the smallest dimension. Once it is greater than 150 µm, the smallest gap between the microlines becomes the limiting factor, and $t_{filling}$ becomes independent of channels' depth. The flow rates achieved in our pumps are reported in Figure 6c, ranging from micro- to nanoliters per second and ensuring no entrapment of air. In summary, this section presents two main results. Firstly, we perform the demonstration of a monolithic microfluidic device made exclusively of a thermoplastic and flexible material, with highly stable hydrophilicity. Secondly, we confirm through reproducible fluid flow studies, qualitatively justified by microfluidic fluid dynamics law, the results of our AFM study, showing that the surface of the material is consistently homogeneous at the microfluidic scale, ensuring a stable fluid interface. Those qualities, together with its low small-molecule absorption, biocompatibility and ability to achieve conformable contact over human skin, makes Flexdym™ a uniquely adequate material for wearable microfluidic diagnostic devices.

4. Conclusion

Using a 30 s isothermal, low-pressure, and non-vacuum-assisted thermoforming process of a novel material, Flexdym™, this study demonstrates an extremely fast microfabrication strategy for the production of microfluidic devices. Employing a simple hot press, this approach also represents an important asset for easier, faster and lower-cost prototyping. Due to the current limitations of prototyping techniques, we believe that our results open new directions for microfabrication developments that are poised to show critical advantages for research activities where numerous chips or multilayered systems are required. For example, Potkay[83] reported the yet unsolved challenges in the development and study of artificial microfluidic lungs, which require the assembly of hundreds of microfluidic foils for the fabrication and testing of clinically-relevant prototypes. In the dominant landscape of microfluidic point-of-care developments, pre-clinical research and validation are also a critical path where current microfabrication approaches face major obstacles. Indeed, for microfluidic applications, the research, validation and qualification of biological performances are essential, and the current lack of optimized prototyping methods is certainly the main impediment for the long-time path from the development of a microfluidic proof-of-concept to an application. In terms of microfabrication properties, the demonstrated performances of our imprint process involving low pressure (<1 bar) represents an opportunity to employ extremely simple press equipment and paves the way for new methods using various master mold materials. Undoubtedly, the fabrication of molds suited to sustain the harsh conditions of standard thermoforming is a hurdle that still represents a tremendous challenge for the scientific community. Compatible with industrial thermoforming techniques, sTPE can therefore be envisaged as a material solution at the research level and toward product developments. Such a seamless strategy is essential, as moving from one material to another within the stream of development is a major difficulty. Indeed, sensitive to the interface properties and related to the assembly procedure, the transfer of diverse biocoating treatments, valving and flow controls and overall performances from one material to another is challenging, time-consuming and in most cases counter-productive.

Regarding the surface properties of Flexdym™ compared to PDMS, we demonstrate the absence of sorption events for the rhodamine dye and its enhanced performance in a live-cell assay. We also highlight the mechanical flexibility and ease of device assembly in the context of several microfluidic skin-patchs, dilutors and capillary pump systems. We further show that the watertight assembly of these devices can be performed without sophisticated equipment and without the need for traditional thermal, solvent or plasma-assisted treatments. Optical and SEM images revealed excellent and defect-free molding performances (of up to 4″ devices) with low-cost SU–8 and epoxy molds. EB soft blocks are the key components that provide reversible up to irreversible bonding properties. Thus, our microfabrication approach can be related to the thermal molding of a *"slow"* adhesive polymer foil, too slow to be bonded onto an inappropriate anti-sticking mold surface, but highly efficient to be bonded on a broad range of others polymer surfaces.

Through AFM investigations and the study of a series of flexible capillary pumps, we also demonstrate that hard PS blocks covalently linked to the EB matrix are evenly arranged on the external polymer surface, providing a homogeneous surface and a stable hydrophilized state upon plasma treatment. Due to the fact that plasma hydrophilization preserves the

mechanical and viscoelastic properties of the Flexdym™ material, it is therefore possible to proceed to the assembly of an entirely plasma-treated capillary pump device without affecting the hydrophilization performances. To our knowledge, this is the first reported solution based on a thermoplastic elastomer material that can be used for fast and reliable assembly while maintaining at the same time a high and stable hydrophilicity.

Finally, the reported strategy and the performances of the proposed material fulfill the major requirements for early prototyping as well as for the development of bioassay protocols. Altogether, the ease of manipulation of Flexdym™, the limited equipment necessary to its patterning, its enhanced performances for bonding and assembly, and the observed limited sorption position this material as a promising solution for the integration of microfluidic devices in a broad range of fields. It bridges the gap between PDMS and current thermoplastic candidates in terms of the benefits for research and product development, combining the advantages of those two material categories in a unique material. Therefore, our work provides a seamless pipeline of microfabrication and bonding from very fast prototyping to high-throughput technologies, bringing clear benefits for microfluidic development and production.

5. Acknowledgments

We thank our colleagues Dominique Decanini, Antoine Pallandre, Anne-Marie Haghiri-Gonest and Christophe David for technical assistance. DC is supported by funding from the European Union's seventh framework program/ERC Grant agreement n°310849. BGE was funded by the Région Bretagne to DC and PYW. ER and DOD acknowledge Catrene (Cluster for Application and Technology Research in Europe for Nanoelectronics), the Spainish Ministerio de Industria, Energía y Turismo, and the French minister of Industry for the financial support of the 3DFF project (3DFF-CT-213/TSI-020401-2012-18). JL, OL and ER are funding from the French national research agency (ANR) as part of the second investissements d'avenir program (BioArtlung Project: ANR-RHUS-0002). CA, IO and LF are supported by the Spanish national research program (BIO2016-79092-R, DPI2015-65401-C3-1-R).

Notes and references

1. K. Ren, J. Zhou and H. Wu, Acc. Chem. Res., 2013, **46(11)**, 2396–406.
2. P. N. Nge, C. I. Rogers and A. T. Woolley, *Chem. Rev. Soc.*, 2013, **113(4)**, 2550–2583.
3. A. Alrifaiy, O. A. Lindahl and K. Ramser, *Polymers*, 2012, **4**, 1349–1398.
4. D. Mark, S. Haeberle, G. Roth, F. von Stetten and R. Zengerle, *Chem. Rev. Soc.*, 2010, **39**, 1153–1182.
5. P. F. O'Neill, A. Ben Azouz, M. Vázquez, J. Liu, S. Marczak, Z. Slouka, H. C. Chang, D. Diamond and D. Brabazon, *Biomicrofluidics*, 2014, **8(5)**, 052112.
6. E. K. Sackmann, A. L. Fulton and D. J. Beebe, *Nature*, 2014, **507**, 181–189.
7. V. Faustino, S. O. Catarino, R. Lima and G. Minas, *Biomechanics*, 2016, **49(11)**, 2280–2292.
8. C. M. Klapperich, *Expert Rev. Med. Devices*, 2009, **6(3)**, 211–213.
9. D. J. Guckenberger, T. E. de Groot, A. M. D. Wan, D. J. Beebe and E. W. K. Young, *Lab Chip*, 2015, **15**, 2364–2378.
10. C. R. Mace and R. N. Deraney, *Microfluid. Nanofluid.*, 2014, **16**, 801–809.
11. J. M. Goddard and J. H. Hotchkiss, Progress in Polymer Science, 2007, **32(7)**, 698–725.
12. H. Becker and C. Gartner, *Anal. Bioanal. Chem.*, 2008, **390(1)**, 89–111.
13. E. Kim, Y. Xia and G. M. Whitesides, *Nature*, 1995, **376**, 581–584.
14. S. K. Sia and G. M. Whitesides, *Electrophoresis*, 2003, **24(21)**, 3563–3576.
15. R. Mukhopadhyay, *Anal. Chem.*, 2007, **79(9)**, 3248–3253.
16. E. Berthier, E. W. K. Young and D. Beebe, *Lab Chip*, 2012, **12**, 1224–1237.
17. J. W. Song and L. L. Munn, *Proc. Natl. Acad. Sci.*, 2011, **108**, 15342–15347.
18. J. S. Gewandter, R. J. Staversky and M. A. O'Reilly, *Free Radical. Biol. Med.*, 2009, **47**, 1742–1752.
19. M. W. Toepke and D. J. Beebe, *Lab Chip*, 2006, **6**, 1484–1486.
20. Y. Tang, E. A. Scheef, Z. Gurel, C. M. Sorensen, C. R. Jefcoate and N. Sheibani, *Am. J. Physiol.: Cell Physiol.*, 2010, **298**, C665–C678.
21. K. J. Regehr, M. Domenech, J. T. Koepsel, K. C. Carver, S. J. Ellison-Zelski, W. L. Murphy, L. A. Schuler, E. T. Alarid and D. Beebe, *Lab Chip*, 2009, **9**, 2131–2139.
22. S. Halldorsson, E. Lucumi, R. Gómez-Sjöberg and R. M. T. Fleming, *Biosensors and Bioelectronics*, 2015, **63**, 218–231.
23. V. Jokinen, P. Suvanto, and S. Franssila, *Biomicrofluidics*, 2012, **6**, 016501.
24. D. T. Eddington, J. P. Puccinelli and D. J. Beebe, *Sens. Actua. B: Chem.*, 2006, **114(1)**, 170–172.
25. S. H. Tan, N.-T. Nguyen, Y. C. Chua and T. G. Kang, *Biomicrofluidics*, 2010, **4**, 032204.
26. D. Ogonczyk, J. Wegrzyn, P. Jankowski, B. Dabrowski and P. Garstecki, *Lab Chip*, 2010, **10**, 1324–1327.
27. E. W. K. Young, E. Berthier, D. J. Guckenberger, E. Sackmann, C. Lamers, I. Meyvantsson, A. Huttenlocher and D. J. Beebe, *Anal. Chem.*, 2011, **83(4)**, 1408–1417.
28. N. Wongkaew, P. He, V. Kurth, W. Surareungchai and A. J. Baeumner, *Anal. Bioanal. Chem.*, 2013, **405(18)**, 5965–5974.
29. T. Hong, W.-J. Ju, M.-C. Wu, C.-H. Tai, C.-H. Tai and L.-M. Fu, *Microfluid. Nanofluid.*, 2010, **9(6)**, 1125–1133.
30. A. Zulfiqar, A. Pfreundt, W. E. Svendsen and M. Dimak, *J. Micromech. Microeng.*, 2015, **25**, 035022.
31. H. Mogi, Y. Fukushi, S. Koide, R. Sano, T. Sasaki and Y. Nishioka, *IEEE Trans. Sens. Micromach.*, 2014, **134**, 366–371.
32. P. S. Nunes, P. D. Ohlsson, O. Ordeig and J. P. Kutter, *Microfluid. Nanofluid.*, 2010, **9(2)**, 145–161.
33. A. B. Azouz, S. Murphy, S. Karazi, M. Vázquez and D. Brabazon,, *Mater. Manuf. Process.*, 2014, **29**, 93–99.
34. C.-W. Tsao and D. L. DeVoe, *Microfluid. Nanofluid.*, 2009, **6(1)**, 1–16.
35. A. Waldbaur, H. Rapp, K. Länge and B. E. Rapp**,** *Anal. Methods***,** 2011, **3**, 2681–2716.
36. E. Roy, M. Geissler, J.-C. Galas and T. Veres, *Microfluid. Nanofluid.*, 2011, **11**, 235–244.
37. M. D. Borysiak, K. S. Bielawski, N. J. Sniadecki, C. F. Jenkel, B. D. Vogt and J. D. Posner, *Lab Chip*, 2013, **13**, 2773–84.
38. D. Brassard, L. Clime, K. Li, M. Geissler, C. Miville-Godin, E. Roy and T. Veres*, Lab Chip*, 2011, **11**, 4099–4107.
39. A. Wasay and D. Sameoto**,** *Lab Chip*, 2015, **15**, 2749–2753.
40. E. Roy, G. Stewart, M. Mounier, L. Malic, R. Peytavi, L. Clime, M. Madou, M. Boissinot, M. Bergeron and T. Veres, *Lab Chip***,** 2015, **15**, 406–416.
41. M. D. Borysiak, E. Yuferova and J. D. Posner, *Anal. Chem.*, 2013, **85(24)**, 11700–11704.
42. E. Roy, M. Mounier, R. Peytavi, J. Siegrist, R. Gorkin, M. Madou, M. G. Bergeron and T. Veres, in *Proceedings of the 14th International conference on miniaturized systems for chemistry and life sciences*, 2010, 1898–1901.
43. A. P. Sudarsan, J. Wang and V. M. Ugaz, *Anal. Chem.*, 2005, **77(16)**, 5167–5173.

44. E. Roy and T. Veres, US Patent 923 8346, 2016, *Microfluidic device, composition and method of forming*. Issued 19th January 2016.
45. M. Zimmermann, H. Schmid, P. Hunziker and E. Delamarche, *Lab Chip*, 2007, **7**, 119–125.
46. http://www.gersteltec.ch/userfiles/1197841293.pdf
47. J. M. Sebastian, C. Lai, W. W. Graessley and R. A. Register, *Macromol.*, 2002, **35**, 2700–2706.
48. J. M. Sebastian, C. Lai, W. W. Graessley and R. A. Register, *Macromol.*, 2002, **35**, 2707–2713.
49. C. M. Sotomayor Torres, *Alternative lithography: unleashing the potentials of nanotechnology*. Kluwer, New York, 2003.
50. S. Florian and I. Novak, *J. Mater. Sci.*, 2004, **39(2)**, 649–651.
51. P. Tordjeman, E. Papon and J.-J. Villenave, *J. Polym. Sci. Part B, Polym. Physic.*, 2000, **38(9)**, 1201–1208.
52. G. Holden, N. R. Legge, R. Quirk and H. E. Schroeder, *Thermoplastic elastomers*, 2nd ed. Hanser/Gardner, Cincinnati, 1996.
53. I. Ochoa I, E. Peña E, E. J. Andreu, M. Pérez-Ilzarbe, J. E. Robles, C. Alcaine, T. López, F. Prósper and M. Doblaré, *J. Biomed. Mater. Res. A.*, 2011, **96(2)**, 341–348.
54. T. Chen, B. Gomez-Escoda, J. Munoz-Garcia, J. Babic, L. Griscom, P.-Y. Jenny Wu and D. Coudreuse, *Open Biol.*, 2016, **6(8)**, doi: 10.1098/rsob.160156.
55. D. Coudreuse and P. Nurse, *Nature*, 2010, **468**, 1074–1079.
56. S. B. Munteanu and C.Vasile, *J Optoelectron Adv Mater.*, 2005, **7**, 3135–3148.
57. B. Morèse-Séguéla, M. St Jacques, J. M. Renaud and J. Prud'homme, *Macromol.*, 1980, **13**, 100–107.
58. V. Studer, A. Pépin and Y. Chen Y, *Appl. Phys. Lett.*, 2002, **80**, 3614–3616.
59. N. S. Cameron, H. Roberge, T. Veres, S. C. Jakeway and H. J. Crabtree, *Lab Chip*, 2006, **6**, 936–941.
60. E. W. K. Young, E. Berthier, D. J. Guckenberger, E. Sackmann, C. Lamers, I. Meyvantsson, A. Huttenlocher and D. J. Beebe, *Anal. Chem.*, 2011, **83(4)**, 1408–1417.
61. A. Mathur, S. S. Roy, M. Tweedie, S. Mukhopadhyay, S. K. Mitra and J. A. McLaughlin, *Curr. Appl. Phy*., 2009, **9**, 1199–1202.
62. H. Odani, K. Taira, N. Nemoto and M. Kurata, *Polym. Eng. Sci*., 1977, **17**,527–534.
63. A. Senuma, *Macromol. Chem. Phys.*, 2000, **201**, 568–576.
64. Y. He, J. Z. Fu and Z. C. Chen, *Microsyst. Technol.*, 2008, **14**, 325–331.
65. M. Worgull and M. Heckele, *Microsyst. Technol.*, 2004, **10**, 432–437.
66. C. Creton, *In: Block Copolymers for Adhesive Applications*, K. Matyjaszewski , Y. Gnanou and L. Leibler (eds),Wiley-VCH, Weinheim, 2007, 1731–1752.
67. G. A. Diaz-Quijada, R. Peytavi, A. Nantel, E. Roy, M. G. Bergeron, M. M. Dumoulin and T. Veres, *Lab Chip*, 2007, **7**, 856–862.
68. Y. Wang, R. Song, Y. S. Li and J.S. Shen, *Surf. Sci.*, 2003, **530**, 136–148.
69. M. Motomatsu, W. Mizutani and H. Tokumoto, *Polymer.*, 1997, **38**, 1779–1785.
70. S. Béfahy, P. Lipnik, T. Pardoen, C. Nascimento, B. Patris, P. Bertrand and S. Yunus, *Langmuir*, 2010, ***26*(5)**, 3372–3375.
71. G. Bar, L. Delineau, A. Hafele and M.-H. Whangbo, *Polymer.*, 1997, **42(8)**, 3627–3632.
72. J. D. Wang, N. J. Douville, S. Takayama and M. ElSayed, *Ann. Biomed. Eng.*, 2012, **40**, 1862–1873.
73. H. Sasaki, H. Onoe, T. Osaki, R. Kawano and S. Takeuchi, *Sens. Actu. B. Chem.*, 2010, **150(1)**, 478–482.
74. G. T. Roman, T. Hlaus, K. J. Bass, T. G. Seelhammer and C. T. Culbertson, *Anal. Chem.,* 2005, ***77*(5)**, 1414–1422.
75. K. Ren, Y. Zhao, J. Su, D. Ryan and H. Wu, *Anal Chem.*, 2010, **82(14)**, 5965–5971.
76. Y. Wang, J. Balowski, C. Phillips, R. Phillips, C. E. Sims and N. L. Allbritton, *Lab Chip*, 2011, **11**, 3089–3097.
77. D. Huh, B. D. Matthews, A. Mammoto, M. Montoya-Zavala, H. Y. Hsin and D. E. Ingber, *Science*, 2010, **328**, 1662–1668.
78. H. J. Kim, D. Huh, G. Hamilton and D. E. Ingber, *Lab Chip*, 2012, **12**, 2165–2174.
79. H. H. Lee, R. A. Register, D. A. Hajduk and S. M. Gruner, *Polym. Eng. Sci.*, 1996, **36**, 1414–1424.
80. D. M. Panaitescu, R. A. Gabor, C. A. Nicolae, M. Ghiurea, M. Mihailescu and R. M. Grigorescu, *Materials & Design*, 2014, **64**, 694–705.
81. F. S. Bates, G. H. Fredrickson, *Ann. Rev. Phys. Chem.*, 1990**, 41**, 525–557.
82. A. Menelle, T. P. Russell, S. H. Anastasiadis, S. K. Satija, and C. F. Majkrzak, *Phys. Rev. Lett.*, **68**, 67–71.
83. J. A. Potkay**,** *Lab Chip***,** 2014, **14**, 4122–4138.
84. D. Juncker, H. Schmid, U. Drechsler, H. Wolf, M. Wolf, B. Michel, N. de Rooj and E. Delamarche, *Anal. Chem.*, 2002, **74(24)**, 6139–6144.
85. L. Gervais and E. Delamarche**,** *Lab Chip***,** 2009, **9**, 3330–3037.
86. J. Berthier, D. Gosselin and E. Berthier, *Microfluid. Nanofluid.*, 2015, **19(3)**, 497–507.
87. E. W. Washburn, *Phys. Rev.*, 1921, **17**, 273–283.